Springer

Journal of
Mechanical
Science and
Technology

Journal of Mechanical Science and Technology 23 (2009) 344~357

www.springerlink.com/content/1738-494x
DOI 10.1007/s12206-008-1116-z

Design and control of a new linear magnetic actuator for squeeze film damper †

Truong Quoc Thanh and Kyoung Kwan Ahn*

School of Mechanical and Automotive Engineering, University of Ulsan, San 29, Muger 2dong, Nam-gu, Ulsan, 680-764, Korea

(Manuscript Received May 16, 2008; Revised November 11, 2008; Accepted November 14, 2008)

Abstract

A new model of a linear magnetic actuator (LMA) that can be applied to the controllable squeeze film damper (CSFD) was proposed, designed, and fabricated. To validate the operation of the proposed actuator, a mathematical model of the proposed LMA was derived through experiments. From the experimental results it was verified that the electromagnetic force depends upon the position of the mover (the outer damper ring of the CSFD) and the applied current. Also, the electromagnetic force varies symmetrically with the position of the mover within the working region. A self-tuning fuzzy PID controller was applied to control the position of the novel LMA. Further, the proposed LMA was assembled in the squeeze film damper (SFD), where the clearance can be controlled by LMA. To investigate the damping effect of the damper under various clearances by controlling the LMA, experiments on the rotor test-rig were conducted. From the experimental results, the proposed device, which is composed of SFD and LMA, was verified to be very effective for attenuation of the vibration of the rotor system.

Keywords: Magnetic actuator; LMA; Moving-magnet; Permanent magnet; Position control; CSFD

1. Introduction

Many kinds of actuators have been developed and widely used in industry. Among them, the magnetic actuator has been considered and studied since the 1960s. However, it has proven to be reliable and flexible in real applications. Recently, many researches have been conducted on magnetic actuators and magnetic effects.

Some mechanical structures and applications of magnetic actuators are presented by Howe [1]. The transverse-flux machine is investigated in [2]; this actuator has promisingly been applied in many applications. In [3], a survey of linear electric actuators, generators and some new configurations of actuators are mentioned and summarized. In references [4-5], the authors investigated a few special types of magnetic actuators via designing, scaling size down, optimizing, and improving the effectiveness of the actuators. Kruusing [7] introduced the magnetic force caused by the reaction between electro-magnet and permanent magnet in the operating area. Danielsson et al. [8] mainly focused on improving the performance of a permanent magnet by using fixation and wave energy conversion in electrical fields through direct drive. Kube et al. [9] presented not only a new configuration of mini-actuator but also the electromagnetic and electro-dynamic force generation principle.

Other studies concentrate on the experimental analysis for investigating the magnetic effect. It has been known that the study of magnetic force is one of the most complex research fields. Besides the theoretical magnetic researches, experiments are required to evaluate the magnetic effects. In [10,11], these impact the experimental studies using permanent magnets and an air track to illustrate dipole-dipole interactions and

† This paper was recommended for publication in revised form by Associate Editor Dong Hwan Kim

*Corresponding author. Tel.: +82 52 259 2282, Fax.: +82 52 259 1680
E-mail address: kkahn@ulsan.ac.kr

mechanical stability. Other researchers [12, 13] investigated the repulsion between two bar magnets which led to the relationship between the distance and the repulsive force. In fact, the interaction force between the two charges is directly proportional to $1/r^2$, $1/r^3$, and $1/r^4$ with respect to monopoles, monopole-dipole, and dipole-dipole, respectively.

The controlling position of the magnetic actuator is required to move the mover accurately; thus a control algorithm is needed to improve the control performance of the actuator. The PID controller has been widely used in industrial control applications. Only three parameters -- the proportional, the integral, and the derivative -- are needed to set the system operation. However, it does not work well in nonlinear systems, high order systems, or time-delay linear systems. To overcome the PID controller restrictions, various modifications to the conventional PID controllers have been made, such as auto-tuning and the development of an adaptive PID controller. In references [14-17], a combination of neural-network/fuzzy and PID constitutes a new type of controller. Simulations and practical examples using the combined controller have been performed to show the superior performance of the combined controller compared to the conventional PID controllers.

A squeeze film damper (SFD) is a special type of bearing, comprising consisting of a journal and a ball bearing. Therefore, SFDs have the advantages of both journals and ball bearings. The journal (called inner damper ring (IDR)) is mounted on the outer race of a rolling element bearing with non-rotation, and the outer damper ring (ODR) is stationary. The annular thin film between the IDR and the ODR, typically less than 0.250 mm, is filled with lubricant. In the operation, the IDR moves as a result of dynamic forces acting on the system and the fluid is displaced to accommodate these motions. The hydrodynamic squeeze film pressures consequently create the fluid forces acting on the journal to attenuate the transmitted forces and reduce the rotor amplitude of motion.

Shafei and Hakim [18] proposed a hybrid squeeze film damper (HSFD). The basic idea is to control the flow in SFD through the movable seals, thus achieving the ability to change the damper from short to long dampers and *vice versa*. A variable geometry with active control logic was implemented. The former configuration is more effective in limiting the transmitted force to the support, because the high damping capacity allows a better reduction of the amplitude response of the rotor. Another work related to the CSFD is also presented by Murthy [19]. In that study, the influence of the working clearance and oil film stiffness of the damper was taken into consideration. Furthermore, the numerical results of the relation amplitude of the shaft versus the rotational speed and film clearance are described by [20]. Recently, SFDs using electro-rheological (ER) and electro-rheological (MR) fluids have been investigated. The ER and MR fluids react to electric and magnetic fields, respectively, and undergo reversible changes in their mechanical characteristics, particularly viscosity and stiffness. A prototype of a directionally controllable SFD, which applies ER fluid to a conventional passive SFD, was proposed by [21, 22]. In references [23, 24], the MR fluid which replaces the lubricating oil in the traditional SFD by controlling the magnetic field to vary the damping of SFD is also presented.

In this paper, a novel LMA and a CSFD are presented with compatible assembly. The LMA is developed to move the ODR of the CSFD. An experimental apparatus for measuring the electromagnetic force of the LMA is established. A mathematic model determines the competence of the actuator's force with assuming that the dependence of magnetic force between two charges proportional to $1/r^2$. Experimental results illustrate the principle of the electromagnetic force with respect to this actuator between the electromagnet and permanent magnet. An advanced control algorithm, which is subsequently applied to control the position of LMA exactly, has proven its effectiveness and reliability in the real applications. Additionally, an experiment of rotor dynamic, combining both LMA and CSFD for reducing the vibration amplitude of the rotor shaft, is also presented.

The rest of this paper is composed as follows: The mechanical model, operating principle and interaction force of the novel LMA are briefly introduced in Section 2. The experiment leading to the mathematical model of the actuator is described in Section 3. Position control of the LMA is presented in Section 4. The application of LMA on CSFD in rotor dynamic behaviour is described in Section 5. Finally, the conclusion summarizes the major findings of this paper.

2. Novel LMA

The LMA consisting of a pair of stator windings is arranged to carry currents for providing magnetic fields with the opposed polarities. The direction of

magnetic flux is arranged as a line which is substantially perpendicular to the directions of current flow in the windings. With a permanent magnet mounted on another actuator's part and opposite magnetic poles with a predetermined spacing, the magnetic effect reacting between electro-magnet and permanent magnet leads to the motion of actuators. To classify the magnetic actuators, there are three basic configurations: moving-coil, moving-iron and moving-magnet. Many mechanical structures and applications of magnetic actuators are presented in the above section. As a consequence, actuators based on the magnetic effect have been developed, effectively applied and still actively researched.

2.1 Mechanical design

The novel LMA is schematically depicted in Fig. 1. It can also be called a moving-magnet linear actuator, though it has a different structure from actuators researched before. The magnetic force, caused by the electrical magnetic effect, is used to control the position of the mover, which can move in a longitudinal direction supported by a set of sliding bearings. Two permanent magnets with opposite poles are mounted on the damper housing. The retaining spring (compressed springs) needs to be installed to back up the damper housing after the de-energizing coil and springs are re-stressed for initial positioning in the middle of the working area. In designing the LMA, it is important that magnetic material cannot be used. Therefore, the mover (consisting of ODR and damper housing) and the IDR are made of non-ferromagnetic material (SUS-304). The air gap between the ends of the U-Shape coil and the permanent magnet is the working area. With this design, if the coil is supplied by a DC current, a magnetic flux will be created between the two ends of the U-shape coil; the magnetic effect between the electro-magnet and permanent magnet then generates the force to move the mover.

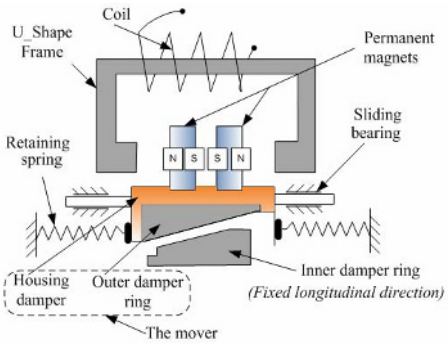

(a). The principle of actuator

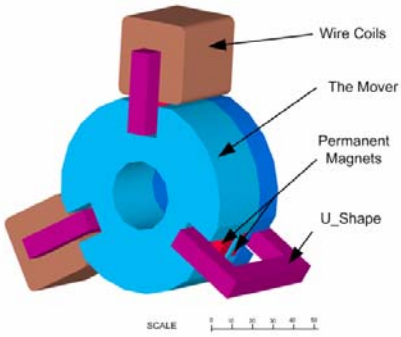

(b). Cad drawing

Fig. 1. Model of novel LMA.

Fig. 2 describes the electromagnetic coil (U-shape), which is made of soft-ferromagnetic material and copper wire 1 mm in diameter with 600 turns. In Fig. 3, the dependence of the electromagnetic poles and the moving direction of the mover in the direction of DC current is shown. Generally, if two magnets with the same poles are brought close to each other, the magnetic force will push the magnets apart. When a DC current with a defined direction is supplied to the coils, the poles of the electro-magnet are defined, which in turn will define the moving direction of the mover as right or left. The magnetic force of LMA is caused from both sides of the U-shape. Both repulsive and attractive forces, therefore, will contribute to the total force. The magnetic effect of the permanent magnet and the electro-magnet causes a magnetic force that acts on the mover. The magnetic flux density of the permanent magnet is constant, whereas that of the electro-magnet is variant. At a defined position, the magnetic force can be changed by tuning the ap-

Fig. 2. The electromagnetic coil (U-shape).

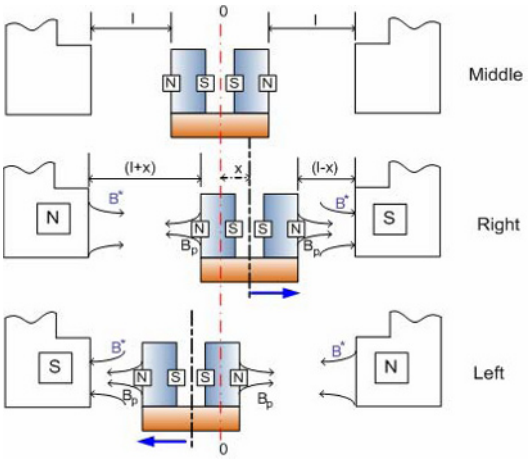

Fig. 3. Moving direction of LMA belong to electromagnetic poles.

plied current. Consequently, the magnetic force of the LMA is partly dependent on the position of the mover and partly dependent on the DC current.

As a result of the movement to the right or to the left of the mover, the clearance of the damper is reduced or extended, respectively. Subsequently, the dynamic characteristic of SFD will be altered due to change of the clearance.

2.2 The interaction force

a. The general magnetic force

Theoretically, the force between two identical cylindrical bar magnets placed end-to-end is given by

$$F = \left[\frac{B_0{}^2 A^2 (L^2 + R^2)}{\pi \mu_0 L^2}\right]\left[\frac{1}{x^2} + \frac{1}{(x+2L)^2} + \frac{2}{(x+L)^2}\right] \quad (1)$$

where

B_0 is the magnetic flux density very close to each pole, *T*

A is the area of each pole, m^2

L is the length of each magnet, *m*

R is the radius of each magnet, *m*

x is the gap between two magnets, *m*

$B_0 = \frac{\mu_0}{2} M$, relates the flux density at the pole to the magnetization of the magnet.

Several formulae for the magnetic force described by Defrancesco and Zaneth (1983) and Romer (1973) are rewritten in Eqs. (2) and (3) as follows*:

$$F = k\left[\frac{1}{(r+h)^2} + \frac{1}{(r+2d)^2} - \frac{2}{(r+d)^2}\right] \quad (2)$$

$$F = k\left[\frac{1}{(x+2b)^2} + \frac{1}{(x+2a-2b)^2} - \frac{2}{(x+a)^2}\right] \quad (3)$$

(*) The coefficients and parameters are defined and used in the reference's paper.

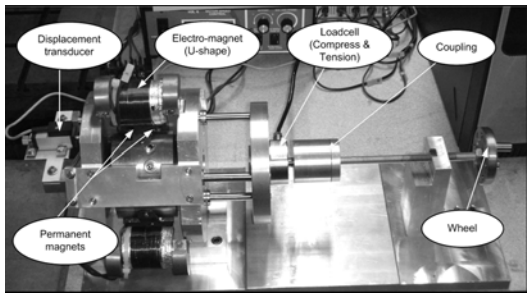

Fig. 4. Test-rig used to measure the magnetic force.

b. An improved electromagnetic force formula.

The magnetic force is influenced by both sides of the mover as mentioned above. At the middle position, the gap between the end of U-shape and the near end of the permanent magnet is *l*(mm). We simplify the formulae in Eqs. (2) and (3), and improve the force formula for the proposed model as below:

$$F = k\left[\frac{1}{(x+b_1)(x+b_2)} + \frac{1}{(x+(a_1+a_2)-(b_1+b_2))^2} - \frac{2}{(x+a_1)(x+a_2)}\right] \quad (4)$$

where

$k(I)$ is the experimental coefficient, relative to DC current, $N.mm^2$

x is the separation of the magnet ends, *mm*

a_1 is the length of permanent magnet, *mm*

a_2 is the alleged length of the electro-magnet, *mm*

b_1 is the distance from the pole to the end of the permanent magnet, *mm*

b_2 is the distance from the pole to the end of the electro-magnet, *mm*.

Regarding the proposed model, at the defined position, x, the magnetic force model can be expressed by its effect on each side of the actuator. Thus, the repulsive and attractive forces are given as follows:

$$F^1_{(I,x)} = k(I)\left[\frac{1}{(l+x+b_1)(l+x+b_2)} + \frac{1}{(l+x+(a_1+a_2)-(b_1+b_2))^2} - \frac{2}{(l+x+a_1)(l+x+a_2)}\right] = k(I)f_1(x) \quad (5a)$$

$$F^2_{(I,x)} = k(I)\left[\frac{1}{(l-x+b_1)(l-x+b_2)} + \frac{1}{(l-x+(a_1+a_2)-(b_1+b_2))^2} - \frac{2}{(l-x+a_1)(l-x+a_2)}\right] = k(I)f_2(x) \quad (5b)$$

with

$|x| \le \delta$, δ is the working region ($\delta < l$).

Consequently, the total electromagnetic force acting on the mover is

$$F^{EM}_{(x,I)} = F^1_{(I,x)} + F^2_{(I,x)} = k(I)\left[f_1(x) + f_2(x)\right] = k(I)f(x) \quad (6)$$

The general form of the electromagnetic force is shown by Eq. (6). This formula is used as the foundation for further experiments to evaluate the working capacity of the LMA.

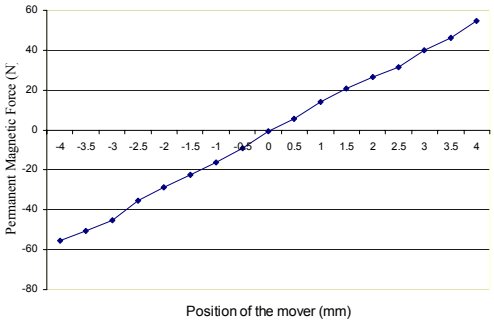

Fig. 5. Experimental magnetic force caused by permanent magnets without applied current.

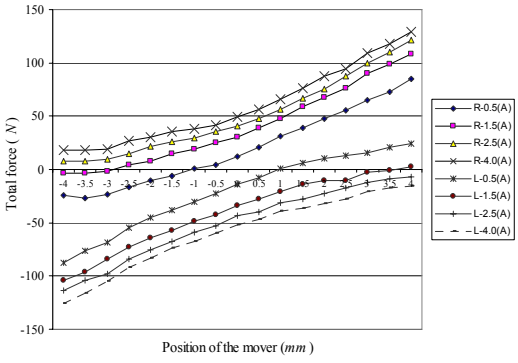

Fig. 6. Experimental total magnetic force relative to applied current and position.

3. Experimental magnetic force of the novel actuator

The experimental apparatus used to measure the balanced force is schematically shown in Fig. 4. The mover is connected to the loadcell (compression and tension), and a screw rod is connected to the loadcell through a flexible coupling. A wheel is fixed at the end of the screw rod to adjust the position of the mover within the operating region. The position of the mover is defined by a displacement transducer (working range is 10 mm). At each position, the force and the position are determined by the loadcell and the displacement transducer, respectively. In general, the forces caused by the reaction of magnets are called the attractive and repulsive force, while the forces acting on the loadcell are called the compressive or tensile force. The electromagnetic force is thoroughly investigated in three stages:

Stage 1: The permanent magnetic force, without supplied current, caused by the permanent magnet and the ferromagnetic material of the U-shape coil, is considered.

Stage 2: The total force from the permanent magnetic and electromagnetic forces is measured at each position of the mover by changing the direction and the magnitude of the applied current (1.0, 2.0, 3.0 and 4.0 amperes).

Stage 3: The experimental data are analyzed and interpolated to derive a general formula for the electromagnetic force.

In stage 1, the permanent magnets acting on the ferromagnetic material are counted by both sides of the mover. When the position of the mover is adjusted by the screw, the relationship between the force and the position is obtained as shown in Fig. 5. As the mover locates at the middle position, the force is balanced, i.e., equals to zero. Otherwise, the force is not balanced and therefore leads to repulsive or attractive forces. According to the interaction forces, if the mover is in the right, the loadcell is compressed and the output signal is positive. If the mover is in the left, the loadcell is tensed and the output signal is negative.

In stage 2, the total force is measured. The force acting on the loadcell in this stage is constituted by the total forces, i.e., both repulsive and attractive forces between the permanent magnets with electromagnet and the soft-ferromagnetic material of U-shape frame are counted to generate the loadcell force.

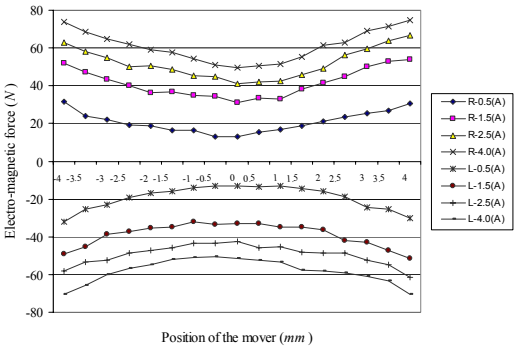

Fig. 7. Electromagnetic force corresponding to the applied current.

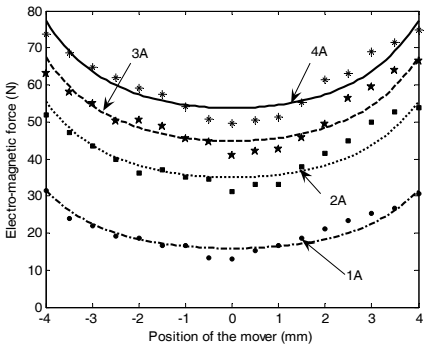

Fig. 8. Electromagnetic force cause the movement in right direction.

The experimental data are achieved by tuning DC current and changing the direction of the applied current. The magnetic effect of the electro-magnet and permanent magnet generates the force acting on the mover. Fig. 6 illustrates the relation between the total force and position of the mover. The direction of the applied current is defined as "*R*" or "*L*" when it causes the movement of the mover to the right or left as presented in Figs. 6 and 7. The magnitude of the total force increased with increasing applied current at the defined position and *vice versa*.

In stage 3, the electromagnetic force, which is calculated by subtracting Fig. 5 from Fig. 6 and caused by the interaction between electro-magnet and permanent magnets, is investigated. This force depends on the applied current and the mover's position which is shown in Fig. 7. The demonstration of the electromagnetic forces belonging to the direction of the applied DC current as defined "*R*" or "*L*" have similar responses in Fig. 7, i.e., the force varies symmetrically and the magnetic force reaches the minimum value at the middle position. Thus, we can consider only the electromagnetic force which tends to cause the mover in the right "*R*" with respect to direction of the applied DC current for investigating the general form, also leading to the mathematical model.

Table 1. The coefficients of the model.

l (mm)	a_1 (mm)	a_2 (mm)	b_1 (mm)	b_2 (mm)
7	5	8	0.5	1

Table 2. The coefficients of interpolated curves.

I (A)	a ($N.mm^2$)	c (N)	$\overline{f(x)\|_{x=-4\div4}}$ (mm^{-2})	$\tilde{k}(I)$ ($N.mm^2$)
1.0	400.1	9.096	0.0275	730.31
2.0	526.8	26.09	0.0275	1473.9
3.0	577.5	35.1	0.0275	1851.7
4.0	601.2	43.55	0.0275	2182.2

The experimental data can be approximately described by curve fitting. The polynomial formed in Eq. (7) is used to fit the experimental data. Fig. 8 presents the curves of an interpolation polynomial with respect to the electromagnetic forces at each applied current.

$$F_{(x,I)}^{EM\_cur1} = a.f(x) + c \tag{7}$$

The electromagnetic force formula can be expressed in the form of Eq. (8) to obtain the coefficient as below:

$$F_{(x,I)}^{EM\_cur2} = \left(a + \frac{c}{\overline{f(x)}\big|_{x=-4\div4}} \right) f(x) = \tilde{k}(I) f(x) \tag{8}$$

where

f(x) is given by the function in Eq. (6), and the coefficients of are given in Table 1; $\overline{f(x)}\big|_{x=-4\div4}$ is the average value of the function *f(x)* in range from -4 to 4; $\tilde{k}(I)$ is the approximate parameter. These coefficients are determined and shown in Table 2.

Figure 9 illustrates the coefficient $\tilde{k}(I)$ corresponding to the DC current. If the solenoid current is variant, the magnetic force will be changed adaptively; the coefficients $\tilde{k}(I)$ (denoted by star points) are inferred from Eq. (8). The interpolation of the cubic polynomial fitting curve is plotted in a continuous line and described by Eq. (9) as below:

$$\tilde{k}(I) = p_1 I^3 + p_2 I^2 + p_3 I + p_4 \quad (9)$$

The parameters in Eq. (9) are: p_1= -5.054, p_2= -52.93, p_3= 838.1 and p_4=-9.967. There is good agreement between the experimental data and the predicted values which are interpolated by the cubic polynomial function. The saturation phenomenon of magnetism causes a considerable decrease of the curve slope for applied currents over 2 amperes; thus the effective applied current on the solenoids is considered less than 2 amperes.

Finally, by substituting Eq. (9) into Eq. (8), the demonstration of magnetic force in a three-dimensional graph is given in Fig. 10. From this graph, it is clear that the magnetic force is sensitively compliant with the applied DC current and the position of the mover. At a defined applied current, the magnitudes of the forces reach the smallest and greatest at the middle and the side position, respectively.

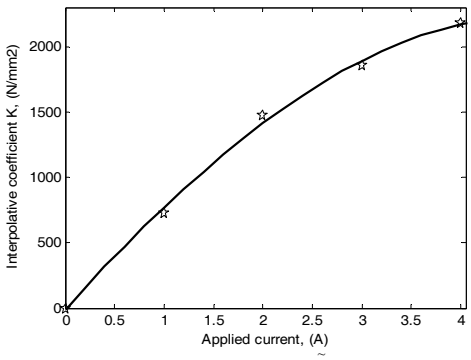

Fig. 9. The experimental coefficient $\tilde{k}(I)$ and the interpolative cubic curve.

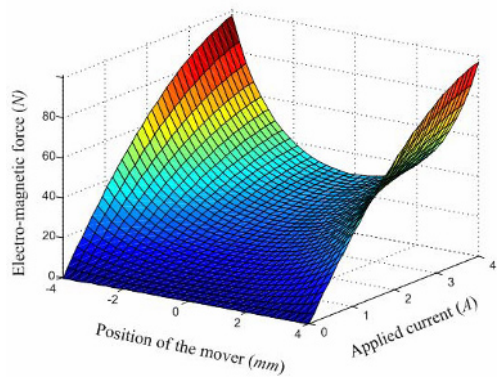

Fig. 10. Electromagnetic force according to the position and applied current.

4. Position control of the LMA

In the previous section, the electromagnetic force was obtained by experiment, and the non-linear behaviour of the model was described. Therefore, this prospect is a basic criterion for choosing the controller, also suitably adjusting the control parameters at each working region. In this section, the structure of a self-tuning fuzzy PID controller is applied to control the actuator.

4.1 Controller design

a. Structure of a self-tuning fuzzy PID controller

The PID controller is widely used in industry due to its simple control structure and easy design. In the time domain, the PID controller can be written as follows:

$$u(t) = K_p + K_d \frac{de(t)}{dt} + K_i \int e(t)dt \quad (10)$$

where $e(t)=y_{sp}(t)-y(t)$ is the system error, $u(t)$ is the control signal, K_p is the proportional gain, K_i is the integral gain, and K_d is the derivative gain. However, certain problems are encountered in practical control systems. The parameters of the conventional PID controller are often not properly tuned for nonlinear plans with unpredictable parameter variations. For this reason, it is necessary to automatically tune the PID parameters. Fuzzy logic can be used to change the PID parameter values during operation. The fuzzy controller provides a formal methodology for representing, manipulating, and implementing heuristic knowledge about how to control a system. This is also a convenient method for constructing nonlinear controllers by using heuristic information obtained from experience. Therefore, the advantages of fuzzy and PID controllers can be combined into a single controller to attain high control performance.

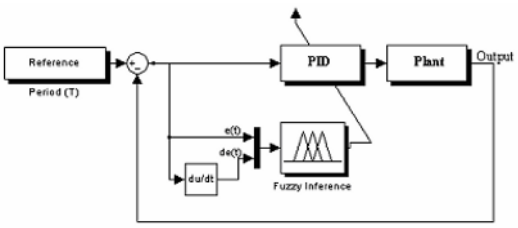

Fig. 11. Structure of self-tuning PID controller.

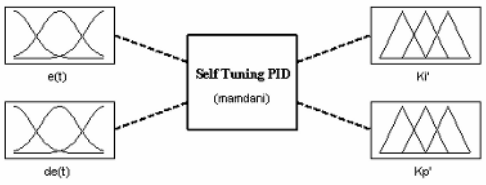

Fig. 12. Structure of the fuzzy inference block.

The structure of a self-tuning PID controller is illustrated in Fig. 11. It has the form of a PID structure with PID parameters that are tuned by fuzzy inference by providing a nonlinear mapping from the signal error *e(t)*, and a derivation of error *de(t)* to the PID parameters K_p, K_i and K_d. These parameters are changed within the initial parameter boundaries. In this paper, for simplicity, but with no loss of reliability, the controller is designed to tune K_p and K_i within the working boundary (Fig. 12).

b. Fuzzy-PID design

Suppose that the variable ranges of K_p and K_i are $[K_{pmin}, K_{pmax}]$ and $[K_{imin}, K_{imax}]$ respectively. In the position control problem of LMA actuators, the range of each PID parameter was experimentally determined as follows: $K_p \in [5, 15]$; $K_i \in [0.5, 4]$, while the derivative K_d is constant (K_d=0.005). To obtain feasible rule bases with high inference efficiency, the PID parameters must be normalized over an interval [0, 1] as follows:

$$K_p^{'} = \frac{K_p - K_{p\min}}{K_{p\max} - K_{p\min}} = \frac{K_p - 5}{15 - 5} \tag{11}$$

$$K_i^{'} = \frac{K_i - K_{i\min}}{K_{i\max} - K_{i\min}} = \frac{K_i - 0.5}{4 - 0.5} \tag{12}$$

We have: $K_p = 10K_p^{'} + 5;\ K_i = 3.5K_i^{'} + 3.5$

The linguistic levels assigned to the input variables [*e(t)* ,*de(t)*] and output variables $\left[K_p^{'}, K_i^{'}\right]$ are as follows:

Neg: negative; Zero: zero; Pos: positive; B: big; M: medium; and S: small.

The control rule-bases deal with the fuzzy rule, {IF A_i and B_i THEN C_i}, as shown in Table 3.

Generally, the fuzzy rules are dependent on the plan to be controlled and the type of controller. These rules are determined from intuition or practical experience. The rule sets are established and shown in surfaces in Fig. 13.

Table 3. Control rule-base.

de \ e	Neg	Zero	Pos
Neg	B	M	B
Zero	M	S	M
Pos	B	M	B

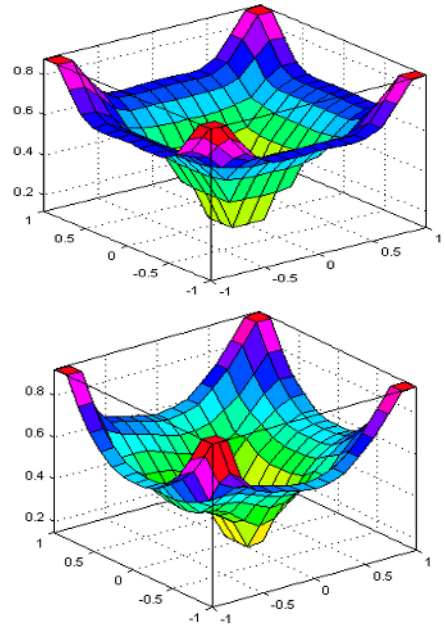

Fig. 13. Fuzzy control rule of $K_p^{'}$ and $K_i^{'}$.

In this paper, the MAX – MIN fuzzy reasoning method is used to obtain output from the inference rule and the present input. For a specific input fuzzy set *A'* in *U*, the output fuzzy set *B'* in O for $K_p^{'}$ is computed through the inference engine as follows:

$$\mu_{B'}(K_p^{'}) = \max_{l=1}^{m}\left[\sup_{x\in U}\min(\mu_{A'}(x), \mu_{A_1^l}(e(t)), \mu_{A_2^l}(de(t)), \mu_{B^l}(K_p^{'}))\right] \tag{13}$$

The output membership function for $K_i^{'}$ is similarly computed. The centroid defuzzification method is used to convert the aggregated fuzzy set to a crisp output value *y** from the fuzzy set *B'* in $V \subset R$. This work computes the weighted average of the membership function or the center of gravity of the area bounded by the membership function curves:

$$y^* = \frac{\int_V \mu_{B'}(y) y dy}{\int_V \mu_{B'}(y) dy} \quad (14)$$

The crisp values of $K_p^{'}$ and $K_i^{'}$ are computed by using Eqs. (11) and (12).

4.2 Experimental results

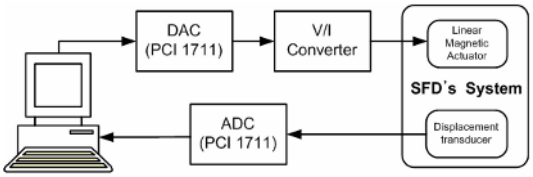

Fig. 14. Experimental apparatus.

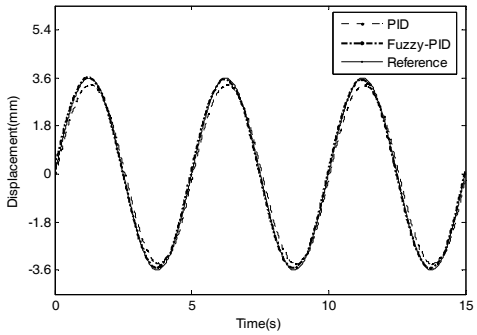

Fig. 15. System response with respect to sine reference input.

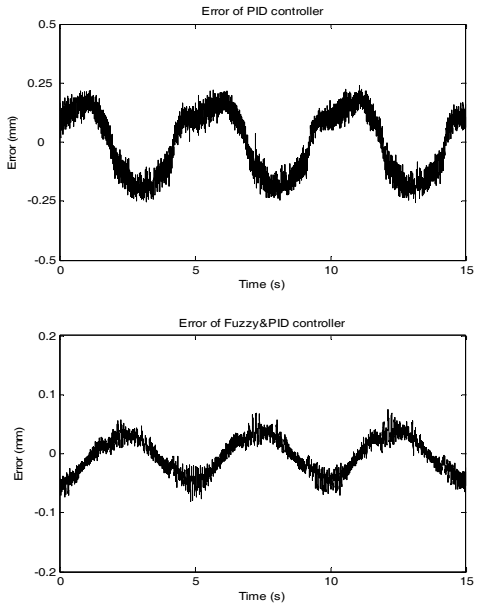

Fig. 16. Steady state error respect to sine reference input.

In Fig. 14, an apparatus is developed to control the position of the mover. The displacement of the mover is measured by a high precision displacement transducer and fed to the computer through an A/D Advantech PCI-1711 card. The performance of the experiment is evaluated by input signals - sine reference. Both the conventional PID and self-tuning fuzzy PID controllers are used.

The PID controller with K_p=10, K_i=2 and K_d= 0.005 represents the conventional PID controller. The experimental results with respect to sine reference are described. The response of the system is shown in Fig. 15. The steady state error and the variant of parameters (K_p, K_i) are shown in Figs. 16 and 17, respectively.

The experimental results demonstrate that the self-tuning fuzzy PID controller is better than the conventional PID controller. Consequently, this controller can be used for moving the ODR of CSFD with more exact position control as well as exact clearance of the damper.

5. Application

5.1 Mechanical assembly

We have proposed a new type of CSFD, with which it is possible to control the radial clearance of the damper by using a novel LMA. The CSFD structure consists of outer and inner damper rings with

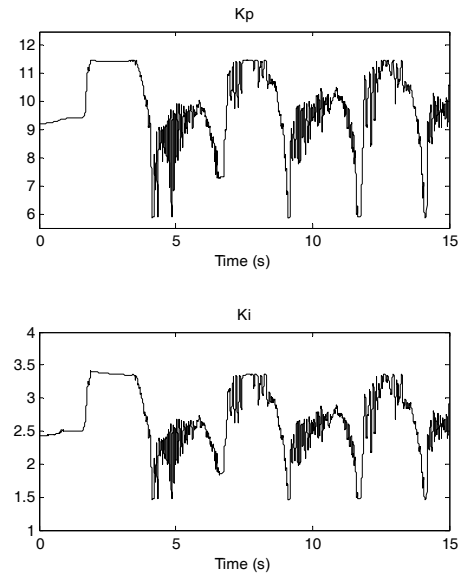

Fig. 17. The changes of K_p and K_i of self-tuning controller.

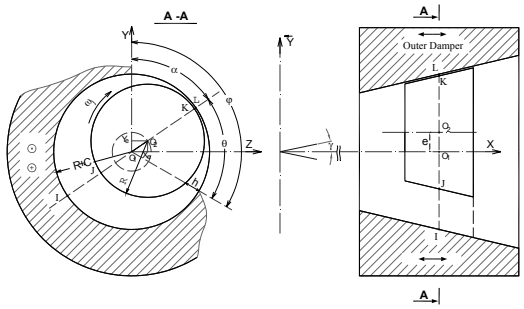

Fig. 18. Controllable squeeze-film damper model.

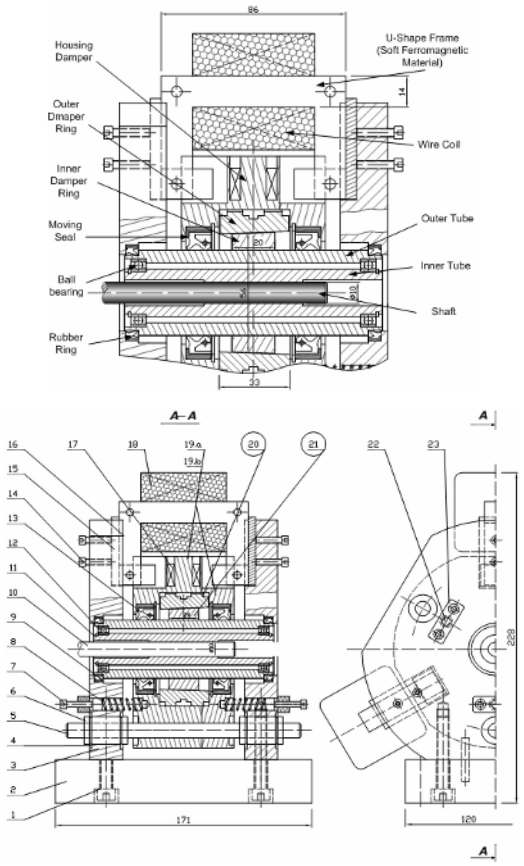

Fig. 19. The LMA is applied to the controllable squeezefilm damper (18. Electro-magnet; 19. Damper housing; 20. ODR and 21.IDR).

conical shapes. A schematic diagram of CSFD is presented in Fig. 18.

The major design consideration in CSFD's configuration is the ability to vary the dynamic behavior of the damper via control of the clearance factor of thin films. Thus, the LMA can effectively control the thickness of fluid film to change the damping force

Table 4. Principal parameters of the SFD.

Electric coil turns	600
Electric coil resistance	2 Ω
Wire diameter	1 *mm*
Radial clearance	50 ÷ 250 μm
Half-conical angle (γ)	2^0
Average diameter of the IDR	55.5 *mm*
Width of the IDR	20 *mm*

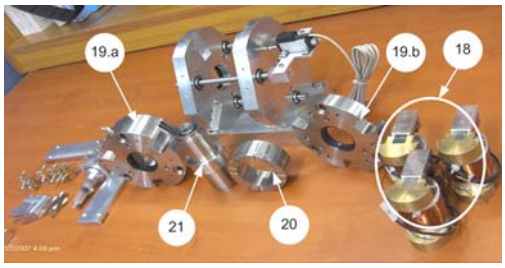

Fig. 20. Realized components of CSFD.

by controlling the position of the ODR. The mechanical design of the CSFD model is illustrated in Fig. 19. The moving housing damper (detail 19), which can be moved in a longitudinal direction by the driving of the LMA, contains the ODR (detail 20) of CSFD. The mover is supported by a set of linear bearings (detail 6). The IDR is restrained in a longitudinal direction by two plastic O-ring springs (detail 9). Three electromagnets with U-shape coils (detail 18) are also described. The area between the IDR and ODR of CSFD creates the radial clearance of fluid film. As a description, if there is relative displacement between the IDR and ODR, clearance of the damper will be determined. The mechanical details of CSFD are fabricated and shown in Fig. 20. The general design parameters of CSFD are 1) inner conical damper of 55.5 mm in average diameter and 20 mm in width, and 2) a half-conical angle γ of 2^0.

5.2 Experiments on SFD

The rotor experimental apparatus, shown in Fig.21, was established by using the Bently Nevada Rotor Kit. It consists of a uniform flexible shaft with length of 400 mm and diameter of 10 mm, an unbalanced mass is mounted on an offset rigid disk (60 g.mm). The shaft is driven by a DC motor, and supported by the journal bearing and CSFD at each end. A flexible coupling is used between the shaft and the motor in order to isolate the vibration transmitted from the

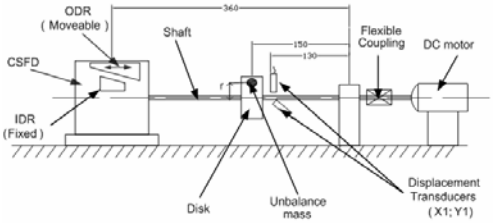

Fig. 21. The experimental schema of the rotor system.

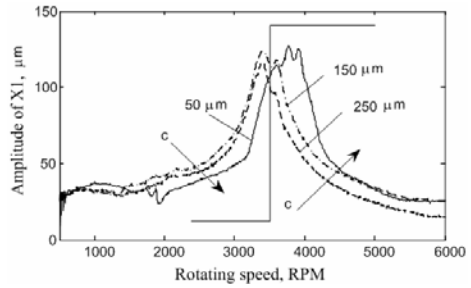

(a). Vibration amplitude of X direction

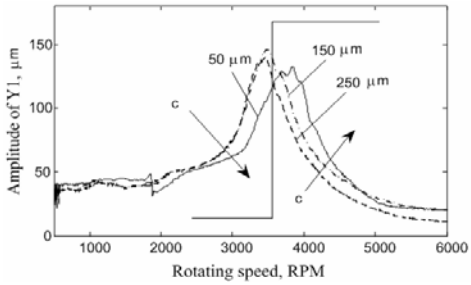

(b). Vibration amplitude of Y direction.

Fig. 22. Steady state response of rotor at position.

motor. The Rotor-Kit has the maximum rotational speed of the DC motor reaching 10,000 rpm, which is equipped with eddy current probes for the relative displacement measurements (3300 NSVTM Probe Proximitor ®). Descriptions of test-rig parameters are denoted in Tables 4 and 5. The movement of the outer damper is in a range of (-2.864 to 2.864 mm) corresponding to the variation of clearance from 50 to 250 μm. The oil used for the test-rig is Shell Tellus 46 (μ=0.0403 Nsm^{-2} and ρ=877 kgm^{-3} at 40^{0}C).

The aim of the experiment was to consider the effect of film thickness on the vibration amplitude of rotor. For investigating the effect of the variation of damping force on the rotor dynamic system response in different working conditions, the experiment was instructed in two cases: Case 1 is the steady-state response; the other case is to apply on-off control to tune the clearance of the damper. The vibration

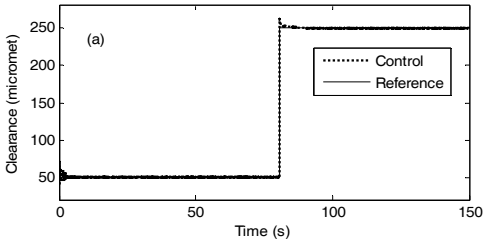

(a). Clearance of the SFD

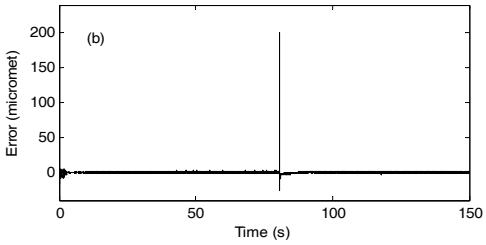

(b). Error signal

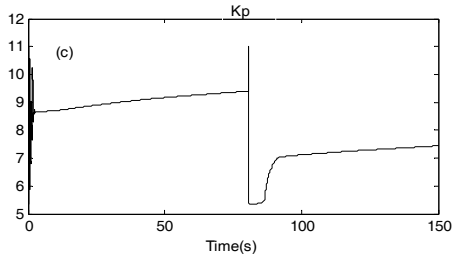

(c). The change of K_p

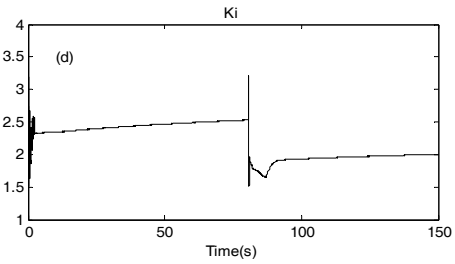

(d).The change of K_i

Fig. 23. Control the clearance of SFD (as the rotor speed reaches 3450 rpm).

amplitude of shaft near the unbalance mass (X1, Y1) is measured by displacement transducers in both horizontal and vertical directions. The measurements could be automatically achieved by the rotor speed run-up on the RAM's reference which is accelerated from 550 to 6000 rpm within 150 seconds for both steady-state responses and on-off control.

Case 1: the steady state response of rotor dynamic. Fig. 22 depicts the relation between the vibration

amplitude of shaft and rotational speed according to the clearance of the SFD in steady-state response. The vibration amplitudes are presented with different radial clearances of 50 μm, 150 μm and 250 μm denoted by continuous, dash-dot and dotted lines, respectively. The first critical speed of the rotor test-rig is about 3230-3900 rpm. The damping force can be varied continuously by controlling the clearance. In detail, as the clearance decreases, the critical speed and critical amplitude slightly increase and *vice versa*.

The experimental results indicate that the vibration amplitude and critical speed depend relatively on the variant of fluid film clearance of the damper. An intersection between the vibration amplitude curves obtained correspondingly to the smallest and largest clearances (50 and 250 μm) is named a critical point. This point is achieved at a rotational speed of about 3450 rpm. To minimize the vibration amplitude of unbalanced mass, on-off control is considered and applied on the rotor system to turn the clearance of the damper as the rotor run-up is passing through the critical point.

Case 2: Control CSFD by ON_OFF. The critical speed testing is the most important before carrying out the application of the control because of the need to verify the behavior of the test-rig. If the run-up rotational speed of the rotor reaches 3450 rpm, the radial clearance will be adjusted from 50 μm to 250 μm by the on-off control. It means that if rotational speed is smaller than 3450 rpm, the smallest radial clearance is selected and *vice versa*. Fig. 23 depicts

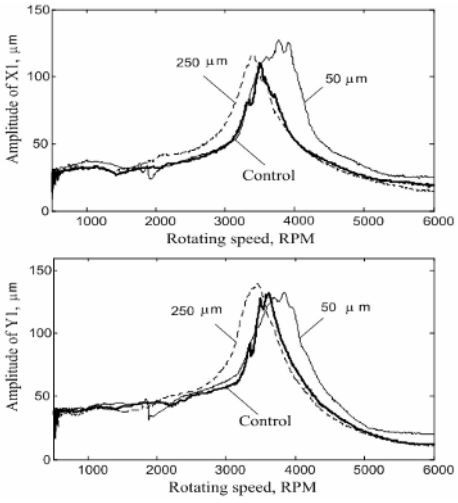

Fig. 24. Control amplitude (X1, Y1) vs. rotational speed.

the control results of the clearance, error and the change of K_p and K_i within 150 seconds as the rotor speed accelerates from 500 to 6000 rpm. The clearance of the damper changes the status from 50 μm to 250 μm within 0.4 second.

Fig. 24 presents the vibration amplitudes of rotor shaft with the applied control. To evaluate clearly the effect of attenuating vibration, we can consider the vibration amplitudes of the rotor at two positions with the rotational speeds at 3200 rpm and 4000 rpm. The correlation of vibration magnitude of unbalanced mass, which could be investigated further by calculating the relative maximum amplitudes between the operating status of the control and the biggest/smallest clearance, is reduced about 32% and 38% at 3200 rpm and 4000 rpm, respectively. It also means that high damping force is necessary as a rotor speed from 550 to 3450 rpm; and low damping force is required as the speed of rotor form 3450 to 6000 rpm. Conclusively, the experiment on SFD indicated that the dynamic behavior of the rotor system is very sensitive by variation of the damper's clearance. The LMA is effectively applied to control the damper leading to attenuating vibration of the rotor system.

6. Conclusions

In our research, both of the novel LMA and CSFD were compatibly designed and investigated. In order to evaluate the reliability of the proposed devices, experiments were conducted in the laboratory. Based on the interaction of magnetic principle, the novel LMA was investigated leading to a mathematical model of electromagnetic force via experimental method. An advanced controller was applied to improve the exactness of the control position of actuator as well as to accurately control the clearance of the damper. Moreover, in rotor dynamic behavior using LMA to control the CSFD, the vibration amplitude of the unbalance mass was considerably reduced via on-off control. This study gives promising prospects not only in applying this type of actuator for future industrial actuator field but also in utilizing the proposed CSFD in rotor dynamic aspects.

Acknowledgment

This research was partly supported by University of Ulsan.

References

[1] D. Howe, Magnetic actuator, *Sensors and Actuator*, Vol. 81 (2000) 268-274.

[2] W. M. Arshad, P. Thelin, T. Backstrom and C. Sadarangani, Use of Transverse-Flux Machines in a Free-Piston Generator, *IEEE Trans. on Industrial Application*, 40(4) (2004) 1092-1100.

[3] I. Boldea and S. A. Nasar, Linear Electric Actuator and Generators, *IEEE Trans. on Energy Conversion*, 14(3) (1999) 712-717.

[4] J. Wang, W.Y. Wang, G.W. Jewell and D. Howe, A Low-Power, Linear, Permanent Magnetic Generator/ Energy Storage System, *IEEE Trans. on Industrial Electronic*, 49(3) (2002) 640-648.

[5] M. Demierre, S. Pesenti, J. Frounchi, P.A. Besse and R.S. Popovic, Reference magnetic actuator for self-calibration of a very small Hall sensor array, *Sensors and Actuators*, A 97-98 (2002) 39-46.

[6] J. Wang, D. Howe and G.W. Jewell, Analysis and Design Optimization of an Improved Axially Magnetized Tubular Permanent-Magnetic Machine, *IEEE Trans. on Energy Conversion*, 19(2) (2004) 289-295.

[7] A. Kruusing, Actuator with permanent magnets having variable in space orientation of magnetization, *Sensors and Actuators*, A101 (2002) 168-174.

[8] O. Danielsson, K. Thorburn, M Erikssion and M. Leijon, Permanent magnet fixation concepts for linear generator, *Fifth European wave energy conference*, (2003) 17-19.

[9] H. Kube, V. Zoeppig, R. Hermann and E. Kallenbach, Electromagnetic miniactuators using thin magnetic layers, *Smart Mater. Struct*., 9 (2000) 336-341.

[10] H.G. Lukefahr, 1992, Magnetic dipole interactions on an air track, *Am. J. Phys*., 60(12) (1992) 1134-1136.

[11] R. Castaner, J.M. Medina and M.J. Cuesta-Bolao, The magnetic dipole interaction as measured by spring dynamometers, *Am. J. Phys.*, 74(6) (2006) 510-513.

[12] S. Defrancesco and V. Zaneth, Experiments on magnetic repulsion, *Am. J. Phys.*, 51(11) (1983) 1023-1025.

[13] A. Romer, Magnetic Repulsion: An Introductory Experiment, *Am. J. Phys.*, 41(12) (1973) 1332-1336.

[14] Y. Yu, Y. Huang, M. Wang, B. Zeng and G. Zhong, Fuzzy Neural PID controller and tuning its weight factors using genetic algorithm based on different location crossover, *Proc. Int. Conf. SMC*, (2004) 3709-3713.

[15] H. Shu and Y. Pi, Decoupled Temperature Control System Based on PID Neural Network, *ACSE 05 Conference, Egypt*, (2005).

[16] K.K. Ahn and B.K. Nguyen, Position Control of Shape Memory Alloy Actuators Using Self-tuning Fuzzy PID Controller, *Int. Journal of Control, ICIEA*, (2006).

[17] R.C. Hwang, H.C. Huang and W.S. Chi, A New Fuzzy PID-Like Controller, *IEEE Int. Conf. on Systems, Man, and Cybernetics*, (2000) 3629-3634.

[18] A. El-Shafei and M. El-Hakim, Experimental investigation of adaptive control applied to HSFD supported rotor, *J. of Eng. For Gas Turbine and Power*, 122 (2002) 685-692.

[19] T.S.R. Murthy, Analysis of multi-scallop self-adjusting conical hydrodynamic bearings for high precision spindles, *Tribology int.*, 14, (1981) 147-150.

[20] O. Bonneau and J. Frene, Non-linear behavior of a flexible shaft partly supported by a squeeze film damper, *Wear*, 206 (1997) 244-250.

[21] Y.K. Ahn, B.S. Yang, and S. Morishita, Directionally Controllable Squeeze Film damper Using Electro-Rheological Fluid, *Transactions of the ASME, Journal of vibration and Acoustics,* 124(1) (2002) 105-109.

[22] S. Morishita and J. Mitsui, Controllable Squeeze Film damper (An application of Electro-Rheological Fluid), *Trans. of the ASME, J. of Vibration and Acoustic*, 114(3) (1992) 354-357.

[23] J. Wang, G. Meng, N. Feng and E.J. Hahn, Dynamic performance and control of squeeze mode MR fluid damper-rotor system, *Smart Materials and Structures*, 14 (2005) 529-539.

[24] P. Forte, M. Paterno and E. Rustighi, A magnetorheological Fluid Damper for Rotor Applications, *Int. J. of Rotating Machinery*, 10(3) (2004) 175-182.

Kyoung Kwan Ahn received the B.S. degree in the department of Mechanical Engineering from Seoul National University in 1990, the M. Sc. degree in Mechanical Engineering from Korea Advanced Institute of Science and Technology (KAIST) in 1992 and the Ph.D. degree with the title "A study on the automation of out-door tasks using 2 link electro-hydraulic manipulator" from Tokyo Institute of Technology in 1999. He is currently a Professor in the School of Mechanical and Automotive Engineering, University of Ulsan, Ulsan, Korea. His research interests are design and control of smart actuator using smart material, fluid power control and active damping control. He is a Member of IEEE, ASME, SICE, RSJ, JSME, KSME, KSPE, KSAE, KFPS, and JFPS.

Truong Quoc Thanh received the B.S degree in the department of Mechanical Engineering from Hochiminh City University of Technology in 1998, and the M.Sc. degree with title "Dynamic stiffness method in calculation vibration of structure" from the master program of mechanics under Inter-University Cooperation Program between Liege University (Belgium) and HCMUT (Vietnam) in 2000. From 2000 to 2004, he worked as a lecturer in the mechanical department of Hochiminh City University of Technology. His teaching subjects are relevant in Advanced Manufacturing Methods, Measuring Technique and Manufacturing Technique. He is currently a Ph.D. candidate at the University of Ulsan. His research interests focus on designing and manufacturing of new actuators, vibration control theory and application theories.